Influence of quantum effects on the physisorption of molecular hydrogen in model carbon foams

A. Martínez-Mesa, S. N. Yurchenko, S. Patchkovskii, T. Heine, and G. Seifert

Citation: J. Chem. Phys. **135**, 214701 (2011); doi: 10.1063/1.3664621
View online: https://doi.org/10.1063/1.3664621
View Table of Contents: http://aip.scitation.org/toc/jcp/135/21
Published by the American Institute of Physics

Influence of quantum effects on the physisorption of molecular hydrogen in model carbon foams

A. Martínez-Mesa,[1] S. N. Yurchenko,[2] S. Patchkovskii,[3] T. Heine,[4] and G. Seifert[2,a)]
[1]*Departamento de Física Teórica, Universidad de la Habana, San Lázaro y L, Vedado, CP 10400, C. Habana, Cuba*
[2]*Institut für Physikalische Chemie und Elektrochemie, Technische Universität Dresden, 01069 Dresden, Germany*
[3]*Steacie Institute for Molecular Sciences, National Research Council of Canada, Ottawa, Ontario K1A 0R6, Canada*
[4]*School of Engineering and Science, Jacobs University Bremen, D-28725 Bremen, Germany*

(Received 27 September 2011; accepted 4 November 2011; published online 5 December 2011)

The physisorption of molecular hydrogen in model carbon foams has been investigated from 50 K to room temperature. The study is carried out within the framework of the density functional theory for quantum liquids at finite temperatures. Calculations are performed in the grand canonical ensemble, i.e., the adsorbed fluid is assumed to be in equilibrium with an external gas of hydrogen molecules with concentrations ranging from 8×10^{-4} kg m^{-3} to $n = 71$ kg m^{-3}. It is shown that, while strong zero-point energy effects are present even at room temperature, the adsorption isotherms exhibit only a weak dependence on the explicit incorporation of the bosonic exchange symmetry of hydrogen molecules. The increase of the average particle density prevents the deviations from the Maxwell-Boltzmann statistics to become noticeable if the system is cooled down. The volumetric storage capacity of these materials at low temperatures is about one half of the U. S. Department of Energy goal, while the gravimetric capacity is still far from the standards required by mobile applications. The relation between the microscopic structure of the hydrogen fluid and the calculated adsorption properties is also addressed. [doi:10.1063/1.3664621]

I. INTRODUCTION

Physical adsorption of molecular hydrogen on nanostructured surfaces has become, during last decades, an active topic of research. The interest on understanding the basic principles behind light molecule adsorption has been triggered by the potential applications of this process to the design and synthesis of efficient hydrogen storage media for fuel-cell driven vehicles, isotope separation via quantum sieving, gas trapping, etc. Many efforts have been addressed, for instance, to the evaluation of hydrogen storage capacity by physisorption on a wide variety of nanostructured materials. Because of their stability, lightweight, and the tunability of their structural parameters, carbon allotropes remain as widespread models of hydrogen storage materials (for a recent review, see Ref. 1). A large number of experimental and theoretical investigations have been devoted to the understanding of the relation between adsorption properties and the structural features of the host media, such as pore size, internal surface area, and topology. Quantum sieving, on the other hand, may provide an alternative way to increase the natural abundance of deuterium other than expensive and energy consuming standard isotope separation techniques such as cryogenic distillation. Theoretical modelling of adsorption plays an important role in the identification of the microscopic mechanisms governing these phenomena, the role of intermolecular interactions in the dynamics and the translation of the measurements into an explicit picture of the molecular spatial distribution.

Quantum effects should be explicitly incorporated in theoretical models of adsorption of light guest molecules such as H_2, this aspect being more relevant in the case of studies of physisorption at cryogenic temperatures.[2–4] For both bulk and confined fluids, the validity of the classical treatment of translational degrees of freedom is usually tested by comparing the de Broglie thermal wavelength $\Lambda = \sqrt{2\pi\hbar^2/mk_BT}$ with the relevant length scales of the system, i.e., the average interparticle distance and the linear dimensions of the trap, respectively. In the case of molecular hydrogen, the de Broglie thermal wavelength varies in the range from 0.7 Å to 1.4 Å when the temperature is reduced from room down to liquid nitrogen temperature. Nevertheless, the use of classical equations of motion for the description of the hydrogen fluid happens to be unjustified already for adsorption in cavities with sizes significantly larger than these values. The reason is that, because of the overlap between the electron densities of the guest molecule and the atoms of the host structure, there is an important fraction of the inner volume that will be inaccessible for H_2 molecules, leading to a restriction of the transverse motion of the particles into a space of effective linear dimensions in the sub-nanometre scale.[5] In presence of this strong confinement, significant differences may arise between theoretical predictions based on quantum-mechanical and classical methodologies due to zero-point energy (ZPE) effects, even at room temperature, as has been found in the case of adsorption in the interstices of nanotubes bundles.[6]

a)Author to whom correspondence should be addressed. Electronic mail: gotthard.seifert@chemie.tu-dresden.de.

The path integral formulation of quantum mechanics provides a suitable statistical mechanical framework for the evaluation of structural properties of quantum many-body systems. At present, numerical implementations of path integral techniques can be grouped in two broad classes: path integral Monte Carlo (PIMC) (Ref. 7) or path integral molecular dynamics (PIMD) (Ref. 8) and their effective potential variant, i.e., the Feynman-Hibbs (FH) approach.[9,10] PIMC and PIMD simulations present the drawback of being computationally demanding even if particle exchange is not explicitly incorporated. On the other hand, molecular dynamics or Monte Carlo calculations based on the FH effective potential have been extensively employed for the computation of static properties of many-body systems because of their lower computational cost. Nevertheless, they are based on a semiclassical approximation of the quantum density matrix and a reliable evaluation of the consequences of such approximation is only available for homogeneous fluids.[11,12] As discussed in Ref. 6, quantum effects might have a significant influence on adsorption at thermodynamic conditions for which they are completely absent in the bulk fluid. Furthermore, at the temperature of liquid nitrogen, the de Broglie thermal wavelength of hydrogen molecules ($\Lambda = 1.40$ Å) is close to the critical value ($\Lambda_c = 1.48$ Å) for the breakdown of the approximation in the uniform system. More accurate hybrid schemes, such as the semiclassical centroid molecular dynamics scheme, require a traditional PIMC or PIMD simulation to retrieve the effective interaction potential between particle centroids at every simulation step[13,14] (or, alternatively, to sample normal modes fluctuations with a short enough period[15,16]).

Suitable alternatives to the above schemes have been developed, based on the application of density functional theory (DFT) to quantum liquids, which allow the computer simulation of quantum many-body systems in equilibrium. These methodologies provide a useful tool for the investigation of the physisorption properties of promising candidate materials for hydrogen storage even in the high density regime, i.e., with large particle counts, and in situations where quantum delocalization effects are dominated by pore confinement instead of the spread of thermal wave packets.

In the present study, we investigate the relevance of both particle delocalization and quantum statistics to the low temperature adsorption behaviour of several carbon foams. Within the quantized liquid density functional theory (QLDFT) introduced in Ref. 17, we evaluate the influence of intermolecular forces on adsorption isotherms. Likewise, we analysed the effects of quantum statistics on the hydrogen adsorption isotherms. While the energy splitting of the allowed hydrogen states is dominated by the confinement imposed by the host nanostructure, the occupation of these levels is given by the different statistics, that is, whether the bosonic hydrogen molecules are treated within the Maxwell-Boltzmann or the Bose-Einstein statistics, and hence one expects different hydrogen density distributions, at least for low temperatures.

Carbon foams constitute allotropes which, by tuning their structural parameters, cover the complete phase space between standard allotropes at ambient conditions of pressure and temperature: diamond and graphite.[18] We concentrate here on a subset of topologies composed of graphite-like (sp^2) segments linked by sp^3 carbon atoms. Atomic coordinates were taken from Kuc and Seifert, who discussed energetics, stability, and mechanical properties of these structures based on density-functional-based tight-binding calculations.[19] In spite of representing the idealized models of real carbon foams, these systems provide a useful insight into the real adsorption mechanism, since multi-walled analogues of these optimized host systems (with similar structural features) have been synthesized already.[20,21] This study focuses on nanostructures with relatively small pore sizes: (n, m) armchair and zigzag foams, with $n = 2, 3$ and $m = 2$, which impose a strong confinement to guest molecules. These non-cylindrical cavities are characterized by an effective radius, defined as the geometrical mean of the largest and the smallest distances to the walls, whose values lie in the range of 3.9 Å–5.4 Å.

The paper is organised as follows. In Sec. II, we briefly describe the methodology employed in the DFT calculations and the way the interactions among guest molecules and with the host structure are modelled. In Sec. III, we present the computed thermodynamic equilibrium properties, the volumetric and gravimetric storage capacities and discuss their relation to the microscopic structure of the hydrogen fluid. Finally, we conclude this work in Sec. IV.

II. METHODOLOGY

The simulations are carried out within the framework of QLDFT, for the fluid composed of featureless hydrogen molecules in the external potential $v_{ext}(\vec{r})$ exerted by the carbon structure on a single H_2 molecule. A detailed description of the theory, together with a discussion of the underlying assumptions and an account of the sparse linear algebra algorithms developed, have been published in Refs. 22 and 17. In the following, we only outline the main ideas and the modifications introduced in order to account for quantum statistical effects on the distribution function of the reference fluid.

The non-interacting reference system is build up by indistinguishable particles obeying Bose-Einstein statistics. For the sake of comparison, the case of particles obeying Maxwell-Boltzmann statistics is also considered. Calculations are carried in the grand canonical ensemble, at constant volume V, temperature T, and chemical potential μ. The spatial density $\rho(\vec{r})$ of the N-body system is evaluated as the corresponding diagonal element of the finite-temperature distribution function of the non-interacting reference fluid,

$$\hat{\rho}_s = f\left[\frac{\hat{H}_s - \mu}{k_B T}\right], \tag{2.1}$$

which minimises the functional,

$$\Omega_{v_{ext}}[\rho] = F_{v_{ext}}[\rho] - \mu \int \rho(\vec{r}) d^3\vec{r}, \tag{2.2}$$

where $F_{v_{ext}}[\rho]$ is the free energy functional of the interacting fluid. In Eq. (2.1), f represents the Bose-Einstein or Maxwell-Boltzmann distribution functions, k_B is the Boltzmann constant, and H_s stands for the effective single-particle Hamiltonian, consisting of the kinetic energy operator and the

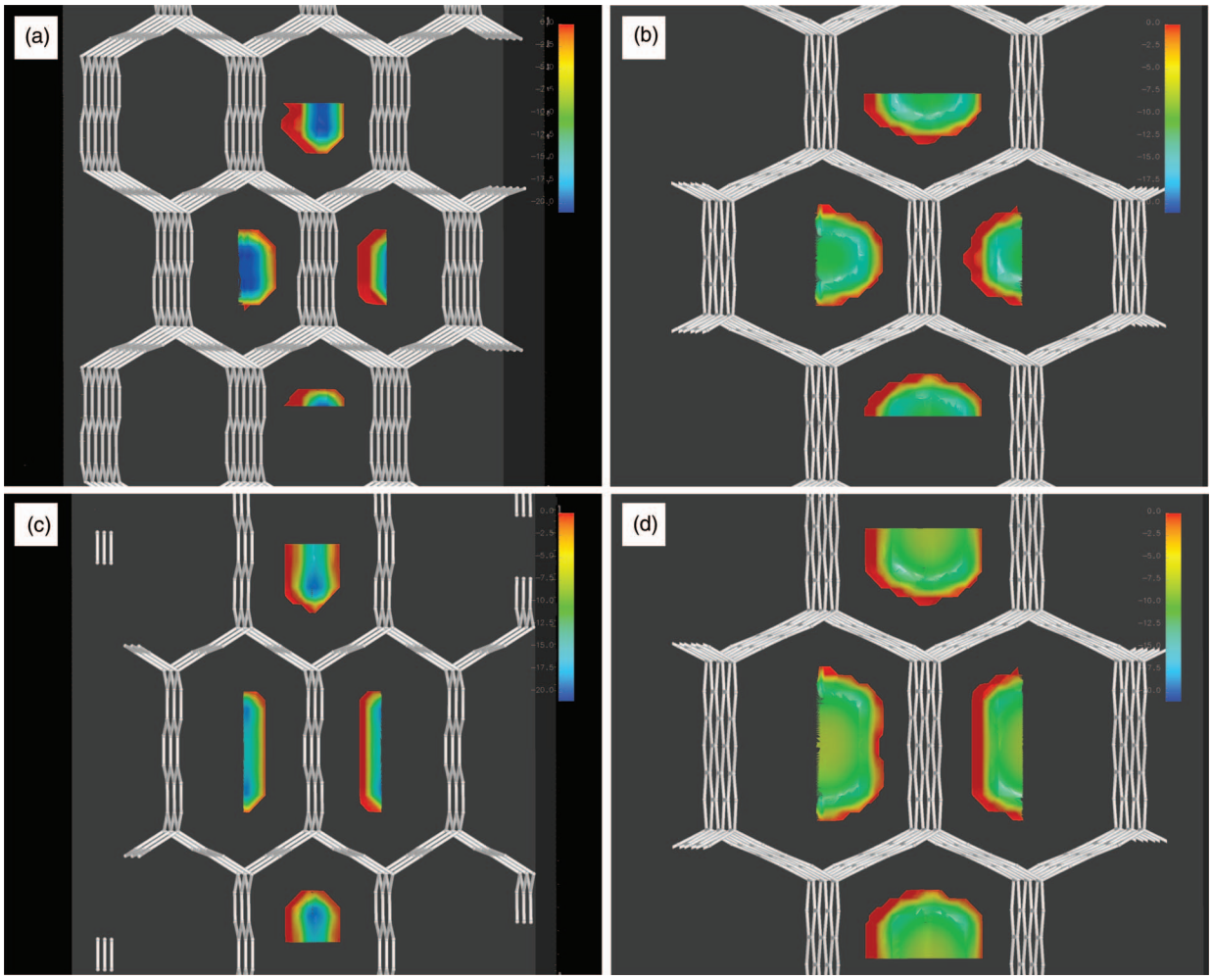

FIG. 1. Contour plots of the interaction potential between H_2 and model carbon foams. The different panels correspond to (a) (2,2) armchair, (b) (2,2) zigzag, (c) (3,2) armchair, and (d) (3,2) zigzag structures. Only the attractive branch of the potential energy surface is shown. The colour scale covers the range from -21 kJ mol^{-1} (blue – the minimum value of the potential exerted by the (2,2) armchair carbon network on a single H_2 molecule) to 0 kJ mol^{-1} (red). The unit cell is replicated along the three spatial directions.

effective potential,

$$v_{eff}(\vec{r}) = v_{ext}(\vec{r}) + \int v\left(|\vec{r} - \vec{r}'|\right) \rho(\vec{r}')d^3\vec{r}' + v_{xc}[\rho(\vec{r})]. \tag{2.3}$$

The potential $v_{ext}(\vec{r})$ is represented through the functional form

$$v_{ext}(\vec{r}) = \sum_i A e^{-a|\vec{r}-\vec{r}_i|} - \frac{C}{|\vec{r} - \vec{r}_i|^6}, \tag{2.4}$$

where summation runs over every carbon atom in the surface and constants are adjusted to fit the post Hartree-Fock calculations carried out on polyaromatic hydrocarbons.[23,24] The external potential v_{ext} is depicted in Figure 1 for the unit cell of the four structures analysed in this work. It can be seen that, for the (2, 2) and (3, 2) armchair frameworks, H_2 molecules experience a nearly two-dimensional localization close to the centre of the cavities, characterized by well depths of 21 kJ mol^{-1} and 19 kJ mol^{-1}, respectively. On the other hand, the (2, 2) and (3, 2) zigzag structures exhibit two broad potential minima with depths of 14.5 kJ mol^{-1} for the former and 13 kJ mol^{-1} in the latter case. For each of these foams, the H_2-surface interaction prevents adsorption in a large fraction of the cavity volume (uncoloured space). Likewise, the corrugation of the potential energy surface comes into sight in the isosurface, indicating the limits of the region where the repulsive branch of v_{ext} dominates.

Since within our approximations H_2 molecules are considered as point particles, the intermolecular interaction $v(r)$ depends only on the separation between their centres of mass. The isotropic average of *ab initio* data points, which reproduces the experimental values of the second virial coefficients in the range of temperatures from 15 K to 500 K,[25] were fitted with a Morse function, the potential parameters being $D = 0.291$ kJ mol^{-1}, $r_e = 3.511$ Å, and $\alpha = 1.592$ Å^{-1}.

The exchange-correlation potential v_{xc} is evaluated from the empirical equation of state for normal hydrogen[26] within the local density approximation according to the procedure described in Ref. 17. The adsorption properties of the (5, 5) zigzag carbon foams have been evaluated for several temperatures ($T = 50$ K, 77 K, 100 K, and 300 K) and concentrations (ranging from $n = 8 \times 10^{-4}$ kg m^{-3} to $n = 71$ kg m^{-3}) of the surrounding gas. The adsorbed fluid is in equilibrium with the latter, so the chemical potential in Eq. (2.1) is

retrieved also from the experimental data of the homogeneous fluid,

$$\mu = \frac{F(p,T)}{N} + \frac{p}{n}, \tag{2.5}$$

where F is the Helmholtz free energy derived from the empirical equation of state[26] for a given pressure p and temperature T.

The computation of the density is carried out through the formal power expansion of the Bose-Einstein distribution function,

$$\hat{\rho}_s = \frac{1}{e^{\beta(\hat{H}_s-\mu)}-1} = \sum_{k=1}^{\infty} e^{-k\beta(\hat{H}_s-\mu)} = \sum_{k=1}^{\infty}\sum_{m=0}^{\infty} \frac{[-k\beta(\hat{H}_s-\mu)]^m}{m!} \tag{2.6}$$

with $\beta = 1/k_B T$. Keeping only the first term in the outer sum, the Maxwell-Boltzmann statistics is recovered. In practice, the sums were cut at $k_{max} = 5$ and $m_{max} = 50$, since those terms were sufficient to achieve convergence in the whole range of temperatures and pressures considered.

We employed a finite-difference representation of the Hamiltonian of the non-interacting reference system on a three-dimensional grid with maximum spacing of $\Delta = 0.4$ Å along each Cartesian axis. Periodic boundary conditions were applied, so the unit cell was replicated along the three spatial directions to evaluate the effective potential (2.3). The full account of optimal simulation parameters, including the handling of linear algebra operations and taking advantage of the sparsity of the Hamiltonian and the density matrix in the finite-difference representation, have been presented in Refs. 22 and 17. The sets of Eqs. (2.1) and (2.3) were solved self-consistently employing a damped stationary-point iterations scheme with a mixing coefficient of 0.15 (Ref. 17) for both density and effective potential fields. Once the number of adsorbed particles (given by the trace of the occupation number operator ρ_s) is evaluated, the equilibrium constant K_e and the volumetric v_{ads} and gravimetric gw storage capacities can be straightforwardly derived,

$$K_e = n_{ads}/n, \tag{2.7}$$

$$v_{ads} = N_A/n_{ads}, \tag{2.8}$$

$$gw(\%) = \frac{100 \cdot n_{ads}}{n_{ads} + \frac{M_C}{M_{H_2}} n_C}, \tag{2.9}$$

where n_{ads} is the average concentration of physisorbed molecules while N_A, M_C, M_{H_2}, and n_C represent the Avogadro number, the mass of a hydrogen molecule, the mass of a carbon atom, and the number density of carbon atoms in the host structure, respectively.

In the bosonic case, the grand potential of the reference fluid is evaluated as the trace of the operator $\hat{\Omega}_s$,

$$\hat{\Omega}_s = -\frac{1}{\beta}\log\left\{\frac{1}{1-e^{-\beta(\hat{H}_s-\mu)}}\right\}, \tag{2.10}$$

which exploits the factorisation of the grand canonical ensemble partition function of non-interacting bosons. A power expansion similar to Eq. (2.6) was employed to represent the operator $\hat{\Omega}_s$,

$$\hat{\Omega}_s = -\frac{1}{\beta}\sum_{k=1}^{\infty}\sum_{m=0}^{\infty} k^{m-1}\frac{[-\beta(\hat{H}_s-\mu)]^m}{m!}, \tag{2.11}$$

while for particles obeying Maxwell-Boltzmann statistics only the terms with $k = 1$ are kept. The classical distribution of H_2 molecules inside the nanostructures was evaluated by setting $k_{max} = 1$ and taking the limit $\beta\hbar^2/(2m\Delta^2) \to 0$ in Eqs. (2.6) and (2.11). In this limit, the spatial distribution obtained reduces to that of classical liquid density functional theory (CLDFT).

III. RESULTS AND DISCUSSION

In Figure 2, we show the computed adsorption isotherms at T= 300 K using both the Bose-Einstein and the Maxwell-Boltzmann distributions to evaluate the particle density using Eq. (2.1). In the latter case, we computed also the average hydrogen density in the unit cell according to CLDFT. It can be assumed that, for this temperature, no noticeable differences arise from the neglect of the bosonic exchange symmetry of H_2 molecules. There is a significant overestimation of the H_2 uptake within the classical treatment for all the structures and external gas pressures considered. For the (2, 2) armchair carbon foam, the volumetric adsorption capacity predicted by the quantum calculations at saturation is 14% smaller than the corresponding classical result. This difference grows for the larger pores, amounting to 18% of the classical density for the (3, 2) zigzag structure. As we will discuss in more detail later, the increase of the deviation between the results of the classical and quantum calculations is due to the larger region available for H_2 inside the (3, 2) zigzag cavity. As a consequence, CLDFT overestimates the adsorbed density over a broader

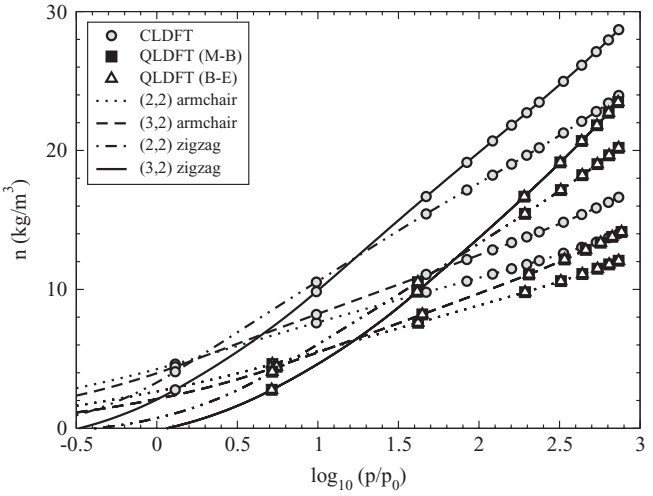

FIG. 2. Average density n of physisorbed molecular hydrogen inside (2,2) armchair (dotted line), (3,2) armchair (dashed), (2,2) zigzag (dashed-dotted-dotted) and (3,2) zigzag (solid) carbon foams, as a function of the external pressure p at $T = 300$ K. p_0 denotes the atmospheric pressure. Adsorption isotherms are calculated within classical liquid DFT (circles) and QLDFT assuming a reference system composed by particles obeying Maxwell-Boltzmann (M-B, black squares) and Bose-Einstein (B-E, up triangles) statistics.

region, and this effect is able to compensate the reduction of the ZPE with respect to the smaller pores. Substantial increase of the pore size will lead, of course, to the vanishing of quantum delocalization effects.

On the (3,2) zigzag carbon network, the amount of physisorbed hydrogen is negligible at atmospheric pressure, i.e., the ZPE of the molecules effectively prevents adsorption on the inner walls of the cavity. On the other hand, classical density functional theory predicts a H_2 concentration of 2 kg m^{-3}, that being a consequence of the value of the chemical potential for the surrounding gas ($\mu(p = 1\text{bar}, T = 77\text{ K}) = -12.5$ kJ mol^{-1}), which is not much lower than the depth of the minimum of the H_2-foam interaction potential. The ratio between the densities of the physisorbed gas computed using the quantum and classical methodologies described above, qualitatively agree with the predictions obtained by PIMC simulations of interstitial adsorption in bundles of (18, 18) carbon nanotubes.[6] Those interstices are characterized by an effective radius of 8 Å, which is similar to the structures analysed in this work.

The direct comparison between the adsorption isotherms and the concentration, predicted for the same thermodynamic conditions, by the empirical equation of state for normal hydrogen[26] allows to establish the range of pressures in which the corresponding carbon structure can be employed to enhance hydrogen storage. At room temperature, this limit ranges from 110 bars to 240 bars, depending on the cavity size. It also fixes the maximum amount of hydrogen that can be efficiently physisorbed on a specific nanostructure (18 kg m^{-3} for the set of carbon arrangements discussed in this paper).

In Figure 3, it can be seen that there is a larger influence of the external potential imposed by the structure on the quantity of physisorbed H_2, when temperature is reduced down to $T = 100$ K. As a consequence, the deviations among the isotherms corresponding to each carbon nanostructure become more striking. Interestingly, the magnitude of quantum effects on the adsorption decreases when the temperature is reduced: in this case the classical predictions are too high by around 9%. This value arises from the competition of the larger population of the lower energy states (compared with the calculations carried out at T= 300 K) and the shift of the latter to higher energies. At $T = 100$ K, more particles will enter the structure to reach the thermodynamic equilibrium between the adsorbed fluid and the external gas, until the increase of the chemical potential $\mu(p, T)$ is balanced by the strengthening of the intermolecular repulsion. As a result of this reinforcement of interparticle interactions, the role played by the potential v_{ext} exerted by the host (and, therefore, by the ZPE) is diminished. At this temperature, the range of pressures that can be used (while keeping the density of molecules adsorbed larger than that of an empty container) gets thinner: up to 44, 53, 86, and 110 bars for the (2, 2) armchair, (3, 2) armchair, (2, 2) zigzag, and (3, 2) zigzag carbon foams, respectively. The maximum value of the average hydrogen density that can be efficiently adsorbed takes the value $n_{ads} = 31$ kg m^{-3}, in the (3, 2) zigzag pores at $p = 110$ bars.

Regarding the possible effects of quantum statistics, it can be seen that, at $T = 100$ K, adsorption isotherms calculated using Bose-Einstein or Maxwell-Boltzmann statistics remain indistinguishable in the whole pressure range. There is a tiny increase (around 0.1%) of the average density if the Bose-Einstein distribution is used. Nevertheless, individual adsorption curves cannot be distinguished within the scale of Figure 3. This is also the case of the isotherms computed at $T = 77$ K, plotted in Figure 4. Essentially the same amount of adsorbed hydrogen is obtained employing a reference system composed by bosons or by particles obeying Maxwell-Boltzmann statistics. Earlier studies also support the idea that Bose-Einstein statistics plays a minor role in quantum fluids at temperatures above 20 K and at typical condensed

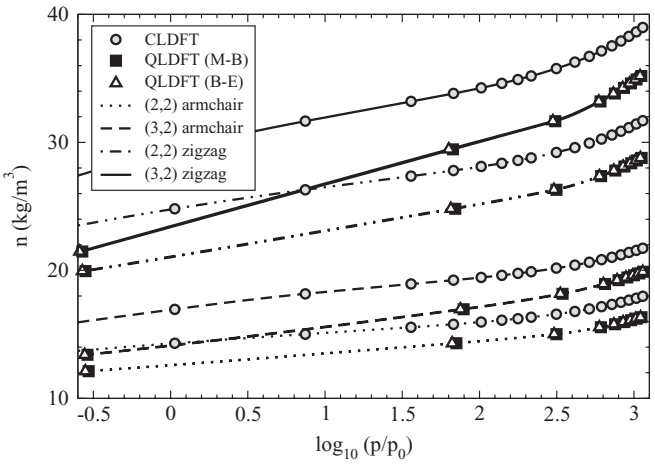

FIG. 3. Adsorption isotherms $n(p)$ for molecular hydrogen inside carbon foams as a function of the external pressure p at $T = 100$ K. p_0 denotes the atmospheric pressure. The dotted, dashed, dashed-dotted-dotted, and solid lines represent the results obtained for (2,2) armchair, (3,2) armchair, (2,2) zigzag, and (3,2) zigzag structures, respectively, which are computed within CLDFT (circles) and QLDFT assuming that H_2 molecules obey Maxwell-Boltzmann (M-B, black squares) or Bose-Einstein (B-E, up triangles) statistics.

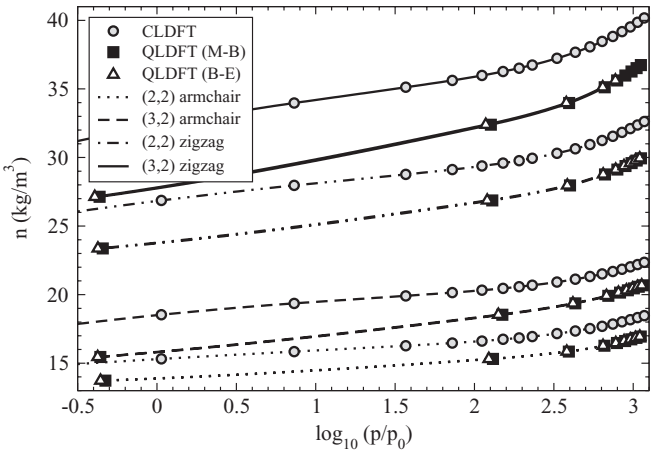

FIG. 4. Concentration n of physisorbed molecular hydrogen inside (2,2) armchair (dotted line), (3,2) armchair (dashed), (2,2) zigzag (dashed-dotted-dotted), and (3,2) zigzag (solid) carbon foams, as a function of the external pressure p at liquid nitrogen temperature $T = 77$ K. p_0 denotes the atmospheric pressure. Adsorption isotherms are calculated within classical (circles) and quantum liquid density functional theories. In the quantum case, black squares and up triangles identify, respectively, the results of calculations employing Maxwell-Boltzmann (M-B) and Bose-Einstein (B-E) statistics.

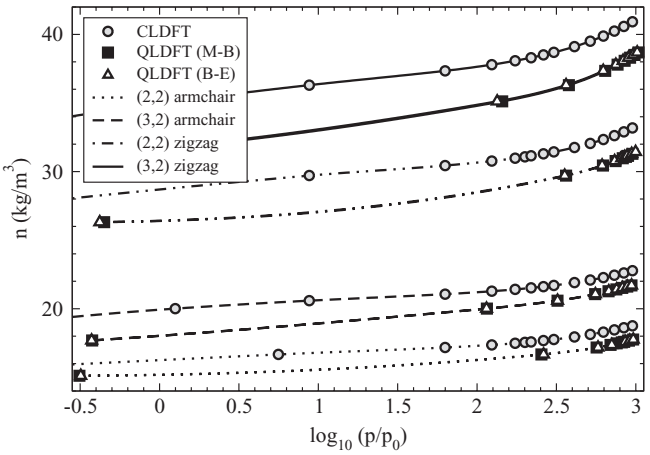

FIG. 5. Average density n of physisorbed molecular hydrogen inside carbon foams as a function of the external pressure p at $T = 50$ K. p_0 denotes the atmospheric pressure. The dotted, dashed, dashed-dotted-dotted, and solid lines represent the results obtained for (2,2) armchair, (3,2) armchair, (2,2) zigzag, and (3,2) zigzag structures, respectively. On the other hand, symbols indicate the results obtained through CLDFT (circles) or whether Maxwell-Boltzmann (M-B, black squares) or Bose-Einstein (B-E, up triangles) statistical distributions were assumed for the reference system in the quantum calculations.

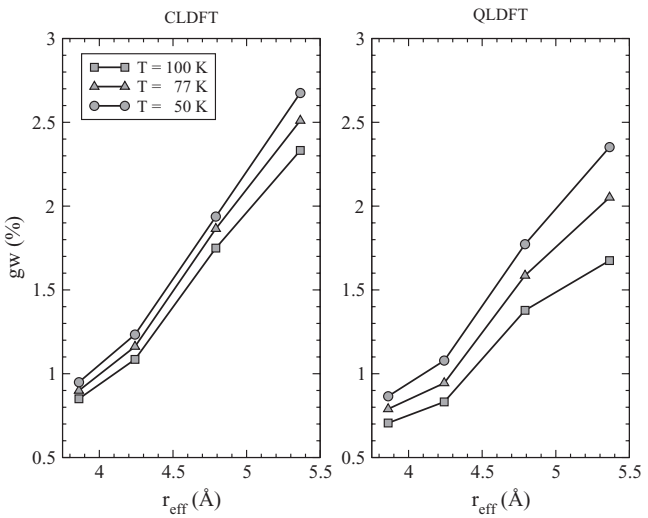

FIG. 6. Gravimetric storage capacities gw at cryogenic temperatures (T = 50 K, 77 K, and 100 K) as a function of the effective cavity radii r_{eff} of carbon foams. The pressure of the external gas is $p = 5$ bars. Outcomes of the classical calculations are shown in the left panel while the results computed within QLDFT are plotted in the right panel.

phase densities. Following a path integral formulation of density functional theory, for example, it has been shown that exchange properties do not have a significant influence on the isotopic shift of the freezing density of helium.[27,28]

At liquid nitrogen temperature, the difference between the concentrations of classical and quantum hydrogen molecules constitutes ~8% of the classical result at saturation pressures. In this case, the presence of the carbon framework will enlarge the density compared to that of hydrogen in free space up to 33 bars (for the (2, 2) armchair) and 85 bars (for the (3, 2) zigzag). For the remaining two nanostructures, the practical pressure limit lies between these values. At the thermodynamic conditions $T = 77$ K, p= 85 bars, the maximum concentration that can be achieved ($n_{ads} = 32$ kg m^{-3}, for the larger cavity) is only slightly larger than the corresponding value at $T = 100$ K and it is about half of U.S. Department of Energy requirement.

In Figure 5, the isotherms corresponding to the lowest temperature investigated ($T = 50$ K). Those curves exhibit prominently fast saturation with the increase of pressure. As a consequence, the set of armchair and zigzag carbon foams analysed here can be efficiently used only for pressures below 30 bars and 65 bars, respectively. At $p = 1000$ bars, the total hydrogen uptakes range from 18 kg m^{-3} to 39 kg m^{-3}, though the largest concentration that can be achieved while retaining a positive excess adsorption density is $n_{ads} = 34.5$ kg m^{-3}. Deviations of the classically calculated densities from those predicted quantum-mechanically take values between 4% and 6% of the former. In contrast, the differences between the calculated Bose-Einstein and Maxwell-Boltzmann isotherms are always below 1%. For every structure, such differences decrease with the growth of the external gas pressure, i.e., with the increase of the average density.

Figure 6 shows the behaviour of the gravimetric storage capacities as a function of the pore sizes at the external gas pressure $p = 5$ bars and at cryogenic temperatures. It can be perceived that, both in classical and quantum calculations, the length scale of the confining potential can be considered as the primary parameter determining the adsorption capacity. The weight percentage of H_2 molecules to the total mass of the system monotonically enlarges as r_{eff} is augmented. By contrast, the gravimetric capacity is not a monotonic function of the specific surface area (SSA). The magnitude of gw is minimal for the (2, 2) armchair network (which has the smallest values of $r_{eff} = 3.9$ Å and SSA = 2816 m^2 g^{-1}) but its value for the (3, 2) armchair ($r_{eff} = 4.2$ Å) is also smaller than for the zigzag frameworks, in spite of having th5e largest specific surface area (4694 m^2 g^{-1}). The largest storage capacities are attained for the zigzag nanostructures (the effective radii are 4.8 Å and 5.4 Å, respectively, for

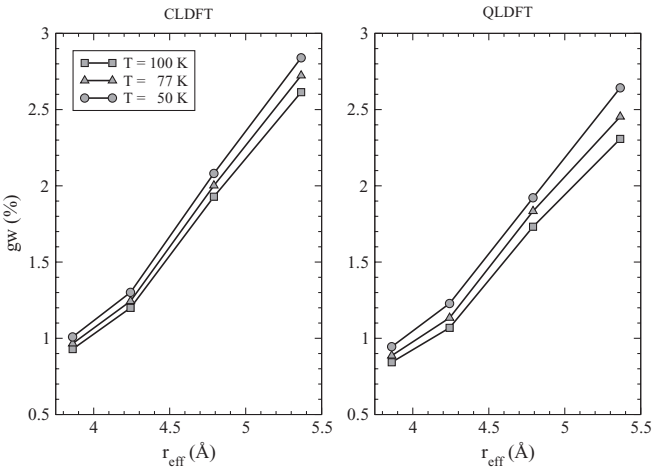

FIG. 7. Gravimetric storage capacities gw at cryogenic temperatures (T = 50 K, 77 K, and 100 K) as a function of the effective cavity radii r_{eff} of carbon foams. The pressure of the external gas is $p = 200$ bars. Outcomes of the classical calculations are shown in the left panel while the results computed within QLDFT are plotted in the right panel.

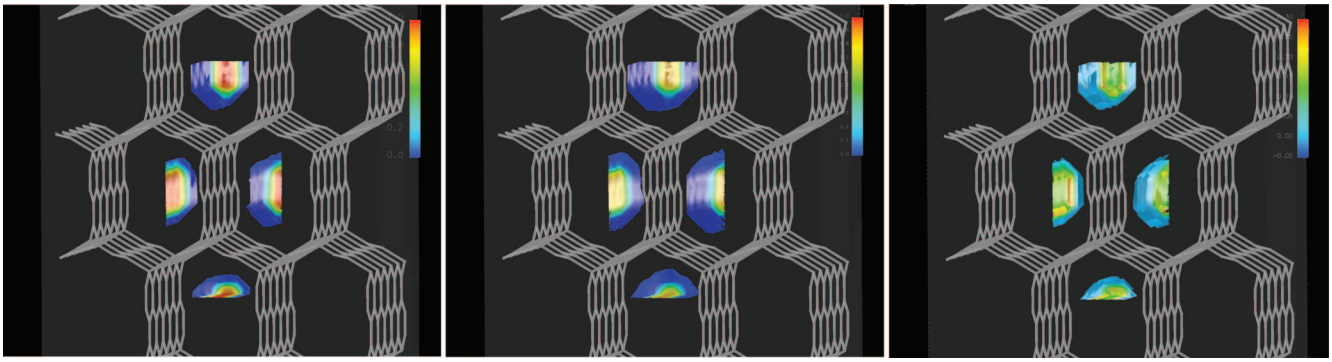

FIG. 8. Surfaces of constant hydrogen density at pressure $p = 10$ bars and temperature $T = 300$ K, inside the unit cell of (2,2) armchair carbon foams. Both the classical (left panel) and quantum (middle) probability densities are shown. On the right, the difference between the classical and quantum densities is depicted. In the first two panels, the colour scale is normalized to the height of the main peak of the classical distribution, while in the right panel the isosurfaces are uniformly distributed between −0.05 and 0.3 times this value.

the (2, 2) and (3, 2) chiralities). Even the highest total weight percentage (≈2.4%) is still far from the technological requirements for mobile applications. It is worth to notice that the average number of particles in the unit cell gets larger while the temperature is reduced at a faster rate if quantum effects are explicitly taken into account, causing the step-down of the classical to quantum differences.

In Figure 7, the classical and quantum storage capacities at moderately high pressures ($p = 200$ bars) are represented. The fast saturation of adsorption properties taking place for the nanostructures investigated in this paper, under cryogenic thermodynamic conditions, is evident. The application of much higher pressures does not lead to significantly larger H_2 uploads with respect to those obtained at $p = 5$ bars. From the results plotted in Figures 6 and 7, it is possible to conclude that the depletion of the gravimetric capacity, as a consequence of the increase of the thermal energy, is less pronounced at high pressures. The weight percentages represented in these pictures are comparable to those reported for other carbonaceous materials.

The distribution of hydrogen molecules in the unit cell of (2, 2) armchair foams, for a hydrogen fluid in equilibrium with an external gas at a pressure $p = 10$ bars and temperature $T = 300$ K, is shown in Figure 8. The colour scale is normalized to the height of the main peak of the classical distribution. Both the classical and quantum spatial distributions of guest molecules are directly related to the main features of the H_2-foam potential energy surface (Eq. (2.4)). In the left panel, hydrogen molecules mainly occupy the centre of the cavity, piling up in a narrow region around the minima of v_{ext}. In the middle panel, it can be appreciated that the quantum distribution is much less structured: the height of the main peak is reduced by about 20%, compared to the classical disposition of H_2 molecules, and presents a longer tail which penetrates the classically forbidden region.

Finally, Figure 9 illustrates the differences in the microscopic density profiles arising from the neglect (left panel) and the consideration (middle) of quantum delocalization effects to build the density matrix of the reference fluid. The plot corresponds to the unit cell of the (3, 2) zigzag carbon foams for the same thermodynamic pressure and temperature of the surrounding gas than in Figure 8. Also in this case, the effect of the confinement on the adsorption sites (located close to the corners of the inner walls) of classical and quantum particles can be clearly appreciated. Main peak depletion and broadening of the quantum distribution are present once more, but they take place over a much broader region. Therefore, the deviations between the total number of adsorbed particles within classical and quantum liquid density functional theories are bigger than for the carbon

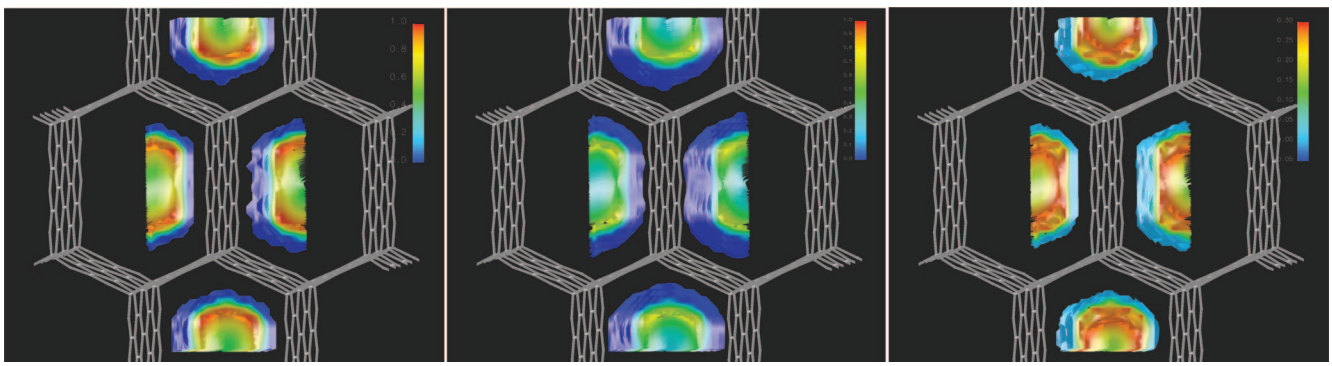

FIG. 9. Spatial distribution of physisorbed hydrogen at pressure $p = 10$ bars and temperature $T = 300$ K, inside the unit cell of (3,2) zigzag carbon foams, shown by means of surfaces of constant H_2 density. Both the classical (left panel) and quantum (middle) density profiles are shown. On the right, the difference between the classical and quantum densities is depicted. In the first two panels, the colour scale is normalized to the height of the main peak of the classical distribution, while in the right panel the isosurfaces are uniformly distributed between −0.05 and 0.3 times this value.

foams with smaller pore size. Moreover, since the quantum density in the space connecting the potential energy surface minima reach almost the same values than at the bottom of the wells, QLDFT predicts preferential adsorption on a ring, in contrast to the classical regime which is characterized by the presence of separated adsorption sites.

IV. SUMMARY AND CONCLUSIONS

We have carried out a study of the adsorption properties of model carbon foam structures explicitly taking into account the quantum nature of the guest molecules via a density functional theory developed for quantum liquids at finite temperature. These hypothetical carbon allotropes are characterized by narrow pores, which impose a strong confinement to the hydrogen fluid. This strong constraint of motion triggers the appearance of non-negligible quantum effects on the physisorption, even at room temperature, as indicated by the differences between adsorption capacities evaluated using classical and quantum density functional theories (which lie between 4% and 18% at high pressures).

These deviations are found to be more pronounced for the (3, 2) zigzag structure, within the set of carbon frameworks studied. The decrease, as the pore size is reduced, of the classical overestimation of the physisorbed H_2 density is caused by diminishing of the area occupied by adsorption sites which compensates the increase of the zero-point energy. The results also show that the disparities between the classical and quantum treatments get thinner as the temperature is decreased, being more severe at $T = 300$ K. Such behaviour is driven by the larger number of particles entering into the structure at lower temperatures. On the other hand, the role of quantum statistics can be fairly neglected for the whole range of thermodynamic conditions investigated. The differences between adsorption isotherms computed by assuming a reference system composed by particles obeying Bose-Einstein or Boltzmann statistics never exceed 1% of the larger concentration for a given pressure and temperature.

Concerning the H_2 adsorption capacities, they both remain far from the technological requirements for efficient hydrogen storage. For temperatures larger than the nitrogen condensation point, none of the analysed carbon frameworks can adsorb molecular hydrogen beyond the following limits: 32 kg m^{-3} or 2.5% of the total mass. It is possible to slightly enhance the H_2 uptake by further pressurization of the external gas, but the resulting concentrations become lower than those that will be achieved in an empty vessel. At cryogenic temperatures, for all the structures considered, both volumetric and gravimetric capacities undergo very fast saturation as the external pressure is augmented.

Furthermore, both classical and quantum distributions of particles inside the unit cell are to great extent determined by the interaction potential between the H_2 molecules and the host structure. As a clear fingerprint, the maxima of the probability densities coincide with the well minima of the confinement potential. The heights of the peaks of the quantum distributions become visibly depleted with respect to the corresponding values calculated within QLDFT. Likewise, quantum density profiles are broader and explore the classically forbidden region. Inside the (3, 2) zigzag carbon foams, classical and quantum densities are characterized by two distinct regimes: the former show independent adsorption sites while the latter is confined on a ring.

As an outlook, we will focus again on the dependence of the concentration of adsorbed hydrogen on the statistical distribution employed to calculate it. The fact that Bose-Einstein and Maxwell-Boltzmann isotherms remain nearly undistinguishable for the whole set of pressures and temperatures examined, poses a question about whether the presence of the nanostructured surface may or may not lead to the observation of marked quantum statistical effects, even at very low temperature. For the present host systems, particle exchange is suppressed by the strong intermolecular interactions taking place at the densities corresponding to the specified thermodynamic conditions. Such depletion will become more severe as temperature gets lower, because of the increase in the particle density. Therefore, it can be foreseen that attempts to progress in the direction of intensifying the role played by Bose-Einstein statistics on adsorption should remain comprised to low-density regimes. Intuitively, the reduction of the interaction strength can be achieved by physisorption on graphene sheets, since the interaction potential between two hydrogen molecules placed at adjacent rings is strongly repulsive ($\approx$6 kJ mol^{-1}). As a consequence, the average distance between molecules that characterizes the low-density physisorption on graphitic platelets is the second neighbours separation (4.2 Å), at which H_2 molecules exhibit a weak attractive interaction. Additionally, the tunability of carbon allotropes provides the possibility to vary the host-H_2 interaction strength, the spacing between neighbouring adsorption sites and the degree of confinement of the motion of the particles into low-dimensionality spaces, in order to enhance quantum statistical effects. Extension of the present work along this route is under way.

ACKNOWLEDGMENTS

A.M.M. acknowledges the financial support from the IMPRS of the Max Planck Institut für Physik komplexer Systeme and from the European Union (EU) project "Inorganic nanotubes and fullerene-like materials."

[1] Y. Yürüm, A. Taralp, and T. Veziroglu, Int. J. Hydrogen Energy **34**, 3784 (2009).
[2] H. Tanaka, J. Fan, H. Kanoh, M. Yudasaka, S. Iijima, and K. Kaneko, Mol. Simul. **31**, 465 (2005).
[3] H. Tanaka, H. Kanoh, M. Yudasaka, S. Iijima, and K. Kaneko, J. Am. Chem. Soc. **127**, 7511 (2005).
[4] A. V. A. Kumar, J. Herv, and S. K. Bhatia, J. Phys. Chem. B **110**, 16666 (2006).
[5] J. J. M. Beenakker, V. D. Borman, and S. Yu. Krylov, Chem. Phys. Lett. **232**, 379 (1995).
[6] Q. Wang and K. Johnson, J. Chem. Phys. **110**, 577 (1999).
[7] D. M. Ceperley, Rev. Mod. Phys. **67**, 279 (1995).
[8] D. Chandler and P. G. Wolynes, J. Chem. Phys. **74**, 4078 (1981).
[9] R. P. Feynmann, and A. R. Hibbs, *Quantum Mechanics and Path Integrals* (McGraw-Hill, New York, 1965).
[10] G. A. Voth, Phys. Rev. A **44**, 5302 (1991).
[11] L. M. Sesé, Mol. Phys. **81**, 1297 (1994).
[12] L. M. Sesé, Mol. Phys. **85**, 931 (1995).
[13] G. A. Voth, Adv. Chem. Phys. **93**, 135 (1996).

[14]H. Saito, H. Nagao, K. Nishikawa, and K. Kinugawa, J. Chem. Phys. **119**, 953 (2003).
[15]J. Cao and G. J. Martyna, J. Chem. Phys. **104**, 2028 (1996).
[16]K. Kinugawa, P. B. Moore, and M. L. Klein, J. Chem. Phys. **106**, 1154 (1996).
[17]S. Patchkovskii and T. Heine, Phys. Rev. E **80**, 031603 (2009).
[18]K. Umemoto, S. Saito, S. Berber, and D. Tomanek, Phys. Rev. B **64**, 193409 (2001).
[19]A. Kuc and G. Seifert, Phys. Rev. B **74**, 214104 (2006).
[20]J. Klett, R. Hardy, E. Romine, C. Walls, and T. Burchell, Carbon **38**, 953 (2000).
[21]J. W. Klett, A. D. McMillan, N. C. Gallego, and C. A. Walls, J. Mater. Sci. **39**, 3659 (2004).
[22]S. Patchkovskii and T. Heine, Phys. Chem. Chem. Phys. **9**, 2697 (2007).
[23]T. Heine, L. Zhechkov, and G. Seifert, Phys. Chem. Chem. Phys. **6**, 980 (2004).
[24]S. Patchkovskii, J. S. Tse, S. N. Yurchenko, L. Zhechkov, T. Heine, and G. Seifert, Proc. Natl. Acad. Sci. U.S.A. **102**, 10439 (2005).
[25]P. Diep and J. K. Johnson, J. Chem. Phys. **113**, 3480 (2000).
[26]R. L. Mills, D. H. Liebenberg, J. C. Bronson, and L. C. Schmidt, J. Chem. Phys. **66**, 3076 (1977).
[27]J. D. McCoy, S. W. Rick, and A. D. J. Haymet, J. Chem. Phys. **92**, 3034 (1990).
[28]S. W. Rick, J. D. McCoy, and A. D. J. Haymet, J. Chem. Phys. **92**, 3040 (1990).